

# UC Davis

## UC Davis Previously Published Works

### Title

Transcription initiation mapping in 31 bovine tissues reveals complex promoter activity, pervasive transcription, and tissue-specific promoter usage

### Permalink

<https://escholarship.org/uc/item/74z980rd>

### Journal

Genome Research, 31(4)

### ISSN

1088-9051

### Authors

Goszczynski, Daniel E  
Halstead, Michelle M  
Islas-Trejo, Alma D  
[et al.](#)

### Publication Date

2021-04-01

### DOI

10.1101/gr.267336.120

### Copyright Information

This work is made available under the terms of a Creative Commons Attribution-NonCommercial License, available at <https://creativecommons.org/licenses/by-nc/4.0/>

Peer reviewed

# Transcription initiation mapping in 31 bovine tissues reveals complex promoter activity, pervasive transcription, and tissue-specific promoter usage

Daniel E. Goszczynski,<sup>1</sup> Michelle M. Halstead,<sup>1</sup> Alma D. Islas-Trejo, Huaijun Zhou, and Pablo J. Ross

Department of Animal Science, University of California, Davis, California 95616, USA

Characterizing transcription start sites is essential for understanding the regulatory mechanisms that control gene expression. Recently, a new bovine genome assembly (ARS-UCD1.2) with high continuity, accuracy, and completeness was released; however, the functional annotation of the bovine genome lacks precise transcription start sites and contains a low number of transcripts in comparison to human and mouse. By using the RAMPAGE approach, this study identified transcription start sites at high resolution in a large collection of bovine tissues. We found several known and novel transcription start sites attributed to promoters of protein-coding and lncRNA genes that were validated through experimental and in silico evidence. With these findings, the annotation of transcription start sites in cattle reached a level comparable to the mouse and human genome annotations. In addition, we identified and characterized transcription start sites for anti-sense transcripts derived from bidirectional promoters, potential lncRNAs, mRNAs, and pre-miRNAs. We also analyzed the quantitative aspects of RAMPAGE to produce a promoter activity atlas, reaching highly reproducible results comparable to traditional RNA-seq. Coexpression networks revealed considerable use of tissue-specific promoters, especially between brain and testicle, which expressed several genes in common from alternate loci. Furthermore, regions surrounding coexpressed modules were enriched in binding factor motifs representative of each tissue. The comprehensive annotation of promoters in such a large collection of tissues will substantially contribute to our understanding of gene expression in cattle and other mammalian species, shortening the gap between genotypes and phenotypes.

[Supplemental material is available for this article.]

With the advent of new sequencing technologies, genomics has emerged as one of the most promising fields in biology. Since its implementation in breeding schemes, livestock industries have seen enormous improvements in productivity (Van Eenennaam et al. 2014), and genomics is expected to play a key role in improving animal welfare, protecting the environment, and securing high-quality food for a growing human population (Britt et al. 2018). For genomic approaches to succeed, high-quality reference genomes are essential. The first bovine genome was published in 2009 (The Bovine Genome Sequencing and Analysis Consortium 2009). Its publication and the improvements that followed have allowed the application of genomic technologies aimed at genetic improvement (Null et al. 2019), the study of molecular and physiological mechanisms of animal health and disease (Ju et al. 2020), and the development of genome engineering approaches (Bevacqua et al. 2016). Recently, a new version of the bovine genome, ARS-UCD1.2, was assembled using single-molecule sequencing, increasing the continuity, accuracy, and completeness compared with its predecessor (Rosen et al. 2020). With a more reliable reference genome available, the focus now transitions from genome sequence to genome features. The annotation of functional regulatory elements in cattle, as well as other important livestock species, is one of the main objectives of the international Functional Annotation of Animal Genomes

(FAANG) Consortium (The FAANG Consortium et al. 2015; www.faang.org).

A key step to study transcription regulation is the elucidation of transcription start sites (TSSs), as these loci harbor transcription factor binding sites that drive gene expression and integrate the inputs from other *cis*-regulatory elements (e.g., enhancers). Generally, TSSs are amid an epigenetic landscape that involves chromatin accessibility (Meers et al. 2018) and H3K4me3 and H3K27ac histone marks (Ernst and Kellis 2017). These epigenetic characteristics can be used to differentiate promoters from other gene regulatory regions, such as enhancers, which are typically enriched in additional histone marks such as H3K4me1 (Ernst and Kellis 2017). Methods to identify 5'-ends of transcripts have been based on the capture of 5' caps or the preferential ligation of adapters to them (Kodzius et al. 2006; Salimullah et al. 2011; Yamashita et al. 2011; Batut et al. 2013), as opposed to RNA-seq methods, in which 5'-ends are frequently underrepresented due to premature termination of reverse transcription (RT), especially when oligo (dT) primers are used. The RNA annotation and mapping of promoters for the analysis of gene expression (RAMPAGE) technique is an accurate 5'-complete cDNA sequencing approach that allows for *ab initio* identification of TSSs at single-base-pair resolution and quantification of their expression (Batut et al. 2013). Briefly, RAMPAGE evaluates statistical enrichment (peaks) of 5' signal

<sup>1</sup>These authors contributed equally to this work.

Corresponding authors: hzhou@ucdavis.edu, pross@ucdavis.edu

Article published online before print. Article, supplemental material, and publication date are at <https://www.genome.org/cgi/doi/10.1101/gr.267336.120>.

© 2021 Goszczynski et al. This article is distributed exclusively by Cold Spring Harbor Laboratory Press for the first six months after the full-issue publication date (see <https://genome.cshlp.org/site/misc/terms.xhtml>). After six months, it is available under a Creative Commons License (Attribution-NonCommercial 4.0 International), as described at <http://creativecommons.org/licenses/by-nc/4.0/>.

across the genome and merges peaks in close proximity to each other into TSS clusters (TSCs). It is worth mentioning that the TSC term was used in the original RAMPAGE publication to refer to the pipeline output, but TSCs are conceptually equivalent to TSSs; in this paper, we will maintain the use of the original nomenclature. In comparison to other protocols, RAMPAGE is simple and scalable, requires low inputs, and allows for discrimination of non-specific signal caused by incomplete cDNAs and of PCR duplicates (Batut et al. 2013).

Considering the start coordinate of an annotated transcript as the TSS, the ARS-UCD1.2 bovine genome annotation from the Ensembl database (release 95) includes 39,705 TSSs for protein-coding or lncRNA transcripts: a low number in comparison to the 139,158 TSSs annotated in human (GRCh38) and the 81,573 TSSs annotated in mouse (GRCm38). Even though small systematic differences are expected in the number of promoters between species, experimental evidence indicates that several bovine transcripts remain to be characterized and annotated (Weikard et al. 2013; Tong et al. 2017). Moreover, studies in mouse and human have shown that a significant proportion of TSSs are enriched in evolutionarily conserved regions (The FANTOM Consortium and the RIKEN PMI and CLST (DGT) 2014; Abugessaisa et al. 2019), suggesting the number of TSSs in the bovine genome should be higher.

As part of the FAANG Consortium, our main objective was to contribute to the bovine transcriptome annotation by identifying TSCs in a large collection of tissues using the RAMPAGE approach. Identified TSCs were validated through several strategies that included experimental evidence from chromatin accessibility assays (ATAC-seq) and histone modification profiling (ChIP-seq), which included H3K4me1, H3K4me3, H3K27ac, and H3K27me3. In addition, we evaluated sequence enrichment for typical promoter elements such as TATA-, GC-, and CCAAT-boxes in regions surrounding TSCs, and known tissue-specific transcription factor binding motifs. The RAMPAGE signal was implemented into a promoter activity atlas that templates transcription initiation in each tissue. To evaluate the quantitative aspect of the technique, we compared it to conventional RNA-seq, which revealed highly consistent and reproducible expression quantification. Unassigned RAMPAGE peaks with insufficient evidence for gene assignment were screened through a set of bioinformatic tools to evaluate their potential as unannotated mRNAs, pre-miRNAs, and ncRNAs. Some of these peaks were particularly interesting due to their antisense activity. Lastly, expression values derived from the RAMPAGE signal were used to generate coexpression networks and to characterize the use of alternative TSCs across tissues.

## Results

### Data set complexity

A total of 111 biological samples corresponding to 31 different tissues from two male (M) and two female (F) individuals were sequenced in nine batches, resulting in 2.72 billion fragments. Most fragments from each library mapped uniquely to the reference genome, yielding a total of 2.39 billion (88%) uniquely mapped fragments (Supplemental Table S1). After duplicate removal, the number of fragments decreased to 673 million (29% of uniquely mapped), with an average of 6.1 million (SD 3.8 million) fragments per sample (Supplemental Fig. S1A). A preliminary evaluation by hierarchical clustering based on gene expression (independent of peak calling) allowed us to identify seven outliers:

abomasum-M1, bladder-F2, colon-F1, esophagus-M1, esophagus-M2, lung-M1, and trachea-M1 (Supplemental Fig. S1B). All outliers were discarded from further analyses. Noise level, measured as the proportion of first reads outside RAMPAGE peaks, was below 20%.

### Identification of TSCs by RAMPAGE

The analysis of 104 samples from 31 tissues from four individuals (two males, two females) identified 93,767 TSCs between the combined data set (87,553) and single-tissue data sets (6214). TSC size varied from a single base to intervals as broad as 1089 bp, with most elements falling in the range of 5–25 bp (Fig. 1A). TSCs identified in the combined data set were supported by a minimum of 22 independent RAMPAGE tags (Fig. 1B), as opposed to tissue-specific TSCs, which were supported by a minimum of three RAMPAGE tags but were conserved between biological replicates.

The bovine genome annotation (Ensembl release 95) considered for this study comprised 33,019 and 31,052 different TSSs and transcription termination sites (TTSSs), respectively, associated with 23,328 protein-coding or long noncoding (lncRNA) genes. To account for nonspecific transcription initiation, TSSs were defined as annotated start coordinate  $\pm 50$  bp. The annotation contained 99 TSSs overlapping with TTSSs, 1676 TSSs overlapping with intron–exon boundaries, and 850 TSSs overlapping with exon–intron boundaries. It is worth mentioning that 662 of the latter overlapped with boundaries at the end of the first exon due to short exon length.

Most of the TSCs identified in this study were absent from the Ensembl annotation. In fact, only 12,072 (13%) of the TSCs overlapped with previously annotated TSSs (Fig. 1C). To determine whether the remaining 19,781 annotated TSSs were undetected or shifted with respect to our findings, we first evaluated their gene expression, and when their expression level was higher than 3 counts per million (CPM), we mapped their location relative to RAMPAGE TSCs. No expression was detected for 3620 (16%) of the annotated genes, which corresponded to 3718 annotated TSSs. The location of the remaining 16,063 nonoverlapped TSSs around TSCs suggested that 44% of these elements were shifted by a margin of 200 bp (Supplemental Fig. S2). No TSC enrichment was observed in the vicinity of TTSSs (Fig. 1D). On the other hand, several TSCs were found to overlap with internal annotated intron–exon (2148) (Fig. 1E) and exon–intron boundaries (299) by at least one base (Fig. 1F).

To evaluate the possibility that boundary-associated TSCs surged as a consequence of transcript fragmentation or capture of partial splicing products, we investigated chromatin accessibility and histone mark profiles in tissues where TSCs were active. This analysis revealed the presence of transcriptional activation marks (H3K4me3, H3K27ac) and accessible chromatin (ATAC-seq) at the TSCs, whereas control intron–exon and exon–intron boundaries showed no enrichment for these marks (Supplemental Fig. S3).

### Assignment of TSCs to genes by sequence evidence

Identified TSCs were assigned to genes based on the alignments of their fragments. We associated 46,708 “genic” TSCs with 18,312 protein-coding and lncRNA genes, accounting for 78% of the 23,328 annotated genes. In addition to these highly associated TSCs, we identified 3789 elements weakly associated with 3176 genes (fewer than three reads), 308 of which were absent from the previous list. Undetected genes were enriched in Gene Ontology (GO) terms associated with olfaction ( $\text{Padj} = 2.6 \times 10^{-165}$ ), taste ( $\text{Padj} = 1.3 \times 10^{-7}$ ), phototransduction

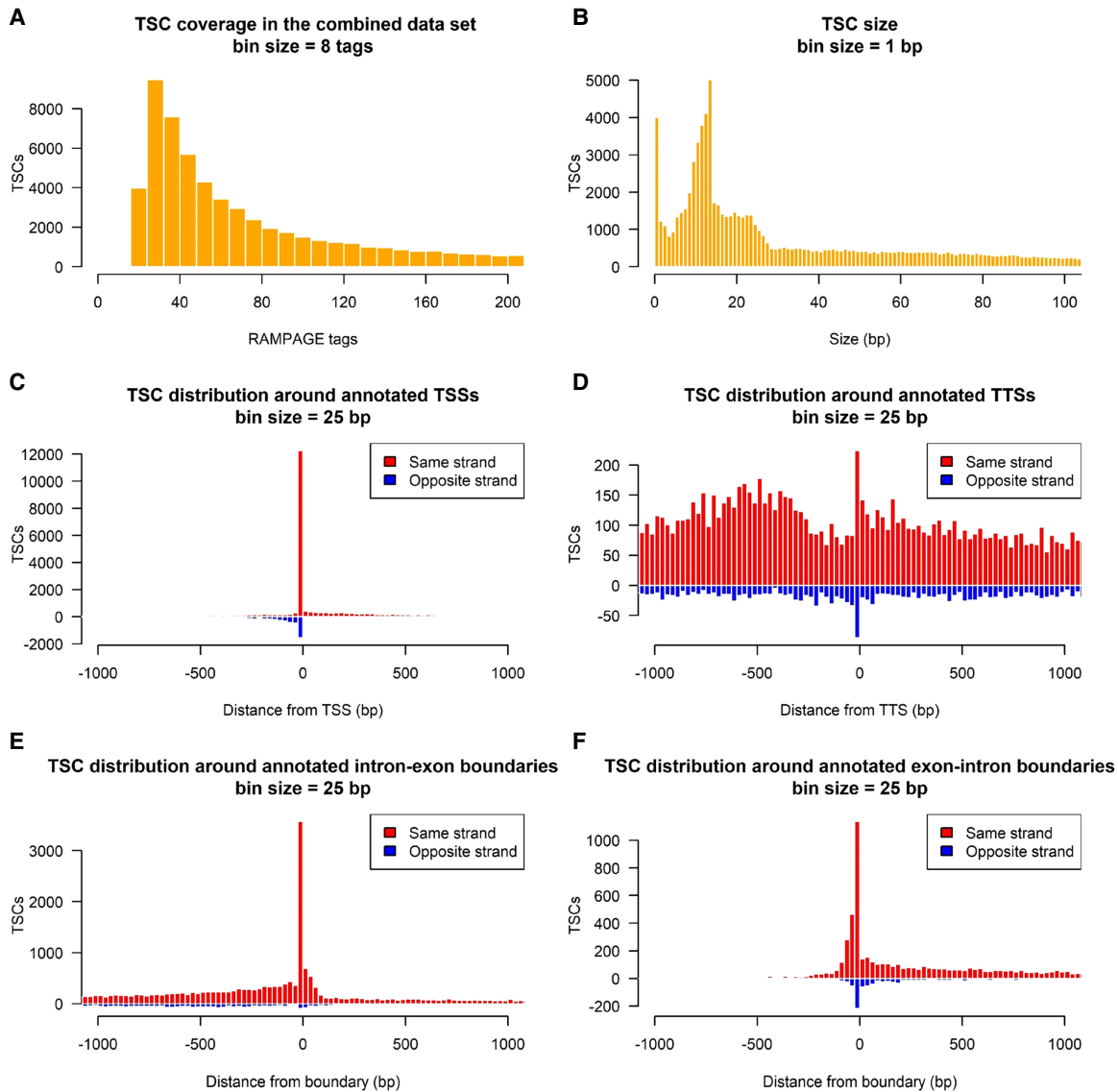


**Figure 1.** Identification of promoters by RAMPAGE. (A) Tag coverage in TSCs identified in the combined data set. (B) TSC size distribution for the whole data set. (C) Histogram of the distance between TSCs and their nearest annotated TSS. (D) Histogram of the distance between TSC and the nearest annotated TTS. (E) Histogram of the distance between TSCs and intron–exon boundaries. Only intron–exon boundaries not overlapping with any annotated TSSs were considered. (F) Histogram of the distance between TSCs and exon–intron boundaries. For visualization, exon–intron boundaries corresponding to the end of the first exon were ignored, as TSCs tended to group immediately upstream of these boundaries and interfere with the visualization.

( $P_{adj} = 9.5 \times 10^{-2}$ ), and defensins ( $P_{adj} = 1.0 \times 10^{-4}$ ). In addition, undetected genes were strongly enriched in homeobox terms ( $P_{adj} = 3.9 \times 10^{-18}$ ), which evidenced the underrepresentation of embryonic and fetal genes in the data set.

The number of genes detected in each biological sample (CPM of genic TSC > 3) varied from 7841 (muscle-M1) to 11,281 (trachea-M2), with an average of 10,009 genes per sample. Based on the Ensembl annotation, 36% of the genic TSCs were located <2.5 kb upstream of annotated TSSs, 31% were in exons, 23% were in introns, and 10% were in intergenic loci (>2.5 kb from annotated TSS) (Fig. 2A). Similar to the global set of TSCs, the size distribution of genic TSCs showed a narrow peak at 1 bp and a broad peak between 5 and 25 bp (Fig. 2B).

The assignment of TSCs to genes revealed that 61% of the detected genes were transcribed from more than one site (Fig. 2C).

We found an average of 2.6 TSC/gene, which was twice the value calculated from the Ensembl annotation (1.3 TSS/gene). Comparatively, our TSC/gene value was between the GRCm38 mouse annotation (2.3 TSS/gene) and the GRCh38 human annotation (2.9 TSS/gene). It is worth mentioning that because RAMPAGE TSCs were identified by merging peaks within windows of 150 bp, we merged annotated TSSs within 150 bp to make comparisons fair.

#### Identification of novel promoters

As mentioned previously, most of the genic transcripts in our data set (34,649) originated from TSCs that were hundreds or thousands of base pairs away from the nearest annotated TSS. To characterize and validate these “novel” genic TSCs, we studied their

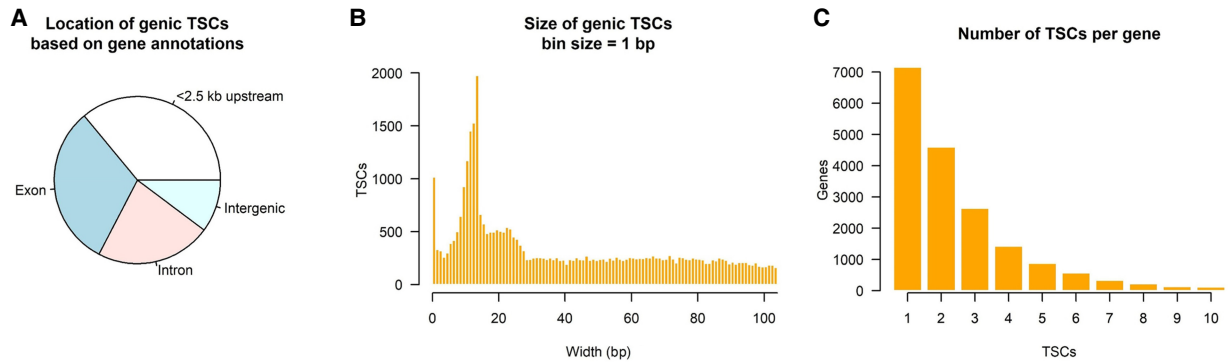


**Figure 2.** Genic TSCs identified by RAMPAGE sequencing. (A) Location of genic TSCs according to gene annotations. (B) Histogram of TSC size. (C) Use of multiple TSCs for the same gene. Genes with more than 10 TSCs were excluded from the plot as they were likely affected by technical artifacts.

location based on gene annotations and their distance to genic TSCs also found in the annotation. Then, we evaluated the presence of typical promoter binding motifs and epigenetic marks for transcriptional activation in regions surrounding TSCs.

According to gene annotations, most of the novel genic TSCs were in exons (38%), followed by introns (30%), regions <2.5 kb upstream of annotated TSSs (18%), and intergenic regions (14%) (Fig. 3A). Novel genic TSCs were abundant within 1 kb upstream of and 2 kb downstream from annotated TSSs (Fig. 3B), constituting new alternative sites for transcription initiation in such genes. In terms of expression, novel TSCs contributed substantially to the transcriptome, with half of them driving >20% of the total gene expression (Fig. 3C).

We then evaluated the characteristics of sequences surrounding novel TSCs (Fig. 3D). We found a high abundance of TATA-boxes 25 bp upstream of novel TSCs, especially for narrow TSCs (Fig. 3E). In general, broad TSCs included more than one TSS, explaining the presence of additional TATA-boxes downstream from the zero coordinate. GC-boxes were highly abundant in broad TSCs and localized mainly at the TSC site and 40 bp upstream. On the other hand, the abundance of CCAAT-boxes was relatively low compared with the other marks, but when present, they localized 10–70 bp upstream of broad TSCs. Binding motif enrichment showed these three motifs were significantly enriched in regions 300 bp upstream of to 100 bp downstream from novel TSCs compared with other sequences from the genome ( $P\text{-value}^{\text{TATA}} = 1 \times 10^{-61}$ ,  $P\text{-value}^{\text{CCAAT}} = 1 \times 10^{-178}$ ,  $P\text{-value}^{\text{GC}} = 1 \times 10^{-183}$ ), as well as regions surrounding internal exons (300 bp upstream to 100 bp downstream;  $P\text{-value}^{\text{TATA}} = 1 \times 10^{-14}$ ,  $P\text{-value}^{\text{CCAAT}} = 1 \times 10^{-14}$ ,  $P\text{-value}^{\text{GC}} = 1 \times 10^{-5}$ ). These data indicated that regions immediately upstream of novel genic TSCs have typical promoter characteristics, validating their identity as TSSs.

By evaluating the chromatin landscape surrounding TSCs, we observed a consistent co-occurrence of enriched chromatin accessibility, H3K4me3, and H3K27ac around novel genic TSCs, indicating these TSCs were associated with an epigenetic signature characteristic of transcriptional activation (Fig. 3F). On the other hand, we detected low signal for H3K4me1 (enhancers) and no signal for H3K27me3 (silencing), which are typically found in enhancers and transcriptionally silent promoters, respectively. Additionally, we observed that the 5' signal at the closest annotated TSS was generally lower and hundreds of base pairs away from the RAMPAGE TSCs (Fig. 3F). Complementarily, we analyzed these epigenetic marks in subgroups of novel genic TSCs classified according to their genic location (exon, intron, intergenic, and pro-

moters), which showed chromatin accessibility, H3K4me3, and H3K27ac enrichment in all subgroups (Supplemental Fig. S4). Overall, the analyzed epigenetic information obtained from chromatin accessibility assays (ATAC-seq) and chromatin immunoprecipitation assays (ChIP-seq) from 12 of the analyzed biological samples indicated that the novel TSCs associated with known genes represented functional TSSs (Fig. 3G).

Some of the novel TSCs in exons showed low epigenetic signal, especially for H3K4me3, suggesting they could represent artifacts produced by RNA degradation or incomplete cDNA synthesis. By generating histograms of the epigenetic signal at these TSCs, we noted a bimodal distribution that separated TSCs into groups with high and low epigenetic signal. By calculating the local minimum of signal, we estimated that ~30% of the novel TSCs in exons were in the latter group and could be potential artifacts (Supplemental Fig. S5). These TSCs were labeled as such in Supplemental Table S2 (see below).

### Unassigned TSCs

Many of the TSCs ( $n=44,125$ ) showed no associations with any annotated lncRNA or protein-coding genes, which could have surged as a consequence of pervasive transcription (Wade and Grainger 2014). Pervasive transcripts are easily distinguished as they are noncoding, not limited by gene boundaries, and frequently antisense, so we proceeded to evaluate such aspects. Unassigned TSCs localized mainly to intergenic (58%) and intronic regions (38%) and were particularly abundant in the vicinity of genic TSCs, but on the opposite strand (Fig. 4A), representing antisense RNA likely generated by bidirectional transcription (Engström et al. 2006). The search for antisense elements in regions 1.5 kb upstream of and downstream from genic TSCs revealed 6946 antisense TSCs associated with genic TSCs from 5247 genes. Sixty percent of these cases occurred within 500 bp upstream of genic TSCs (Fig. 4B), which is consistent with previous observations in the mouse (58%) (Lepoivre et al. 2013). Some of these antisense TSCs were highly correlated with their sense complements, suggesting they were regulated by the same promoter (Fig. 4C). In terms of expression, antisense TSCs generally contributed substantially fewer transcripts than sense TSCs (Fig. 4D). In addition to antisense TSCs in proximity to sense TSCs, we identified 6342 antisense TSCs in gene bodies, resulting in 13,942 antisense TSCs in total and accounting for 30% of the unassigned TSCs.

To further characterize the remaining unassigned TSCs, we generated partial transcript models (Supplemental File S1) and

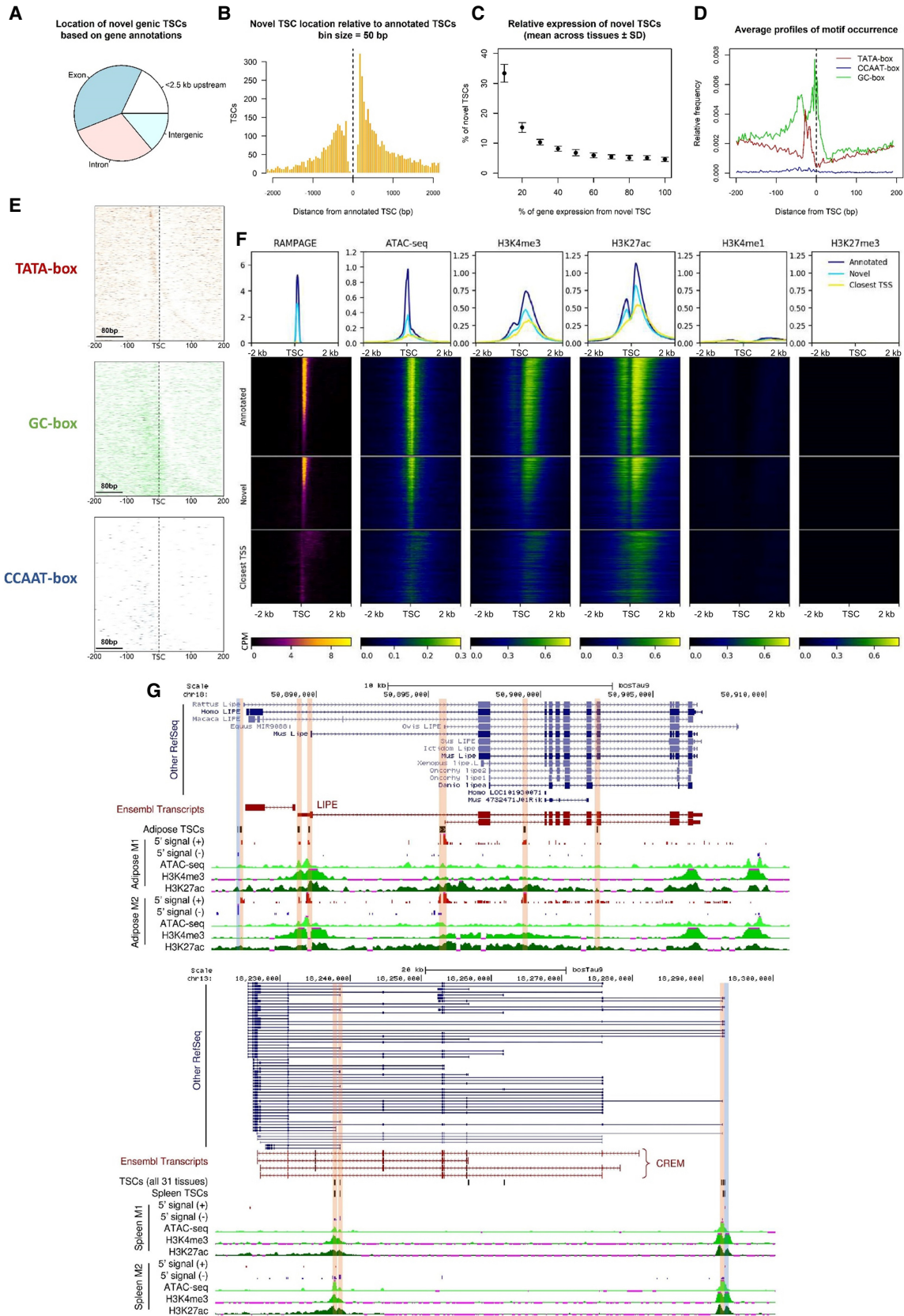


**Figure 3.** Novel promoters identified by RAMPAGE. (A) Location of novel TSCs according to gene annotations. (B) Histogram of the distance between novel TSCs and annotated TSCs. (C) Relative expression of novel TSCs. (D) Profiles of motif occurrence for TATA-, CCAAT-, and GC-boxes around novel TSCs ( $\pm 200$  bp). (E) Motif density maps for TATA-, CCAAT-, and GC-boxes around novel TSCs ( $\pm 200$  bp). TSCs are ordered ascendingly by size; that is, upper rows represent narrow TSCs. The zero coordinate represents the 5'-end of the TSC. Narrow TSCs were particularly enriched with TATA-box motifs and broad TSCs were enriched with GC-box motifs. (F) Epigenetic marks at reported and novel TSCs. The co-occurrence of chromatin accessibility and transcriptional activation marks (H3K4me3, H3K27ac) at novel TSCs, as well as the absence of poised enhancer and repressive marks (H3K4me1, H3K27me3), suggested these TSCs constituted promoter regions. The fuzzy signal observed around the closest annotated TSSs evidenced the absence of annotation for these novel elements. The data shown in the figure correspond to the lung-M2 sample ( $>3$  CPM). Heatmaps are colored according to CPM values. (G) Novel TSCs for the *LIPE* and *CREM* genes. Most of the new variants are supported by annotations from other species. Antisense TSCs were marked with blue to distinguish them from sense TSCs (orange).

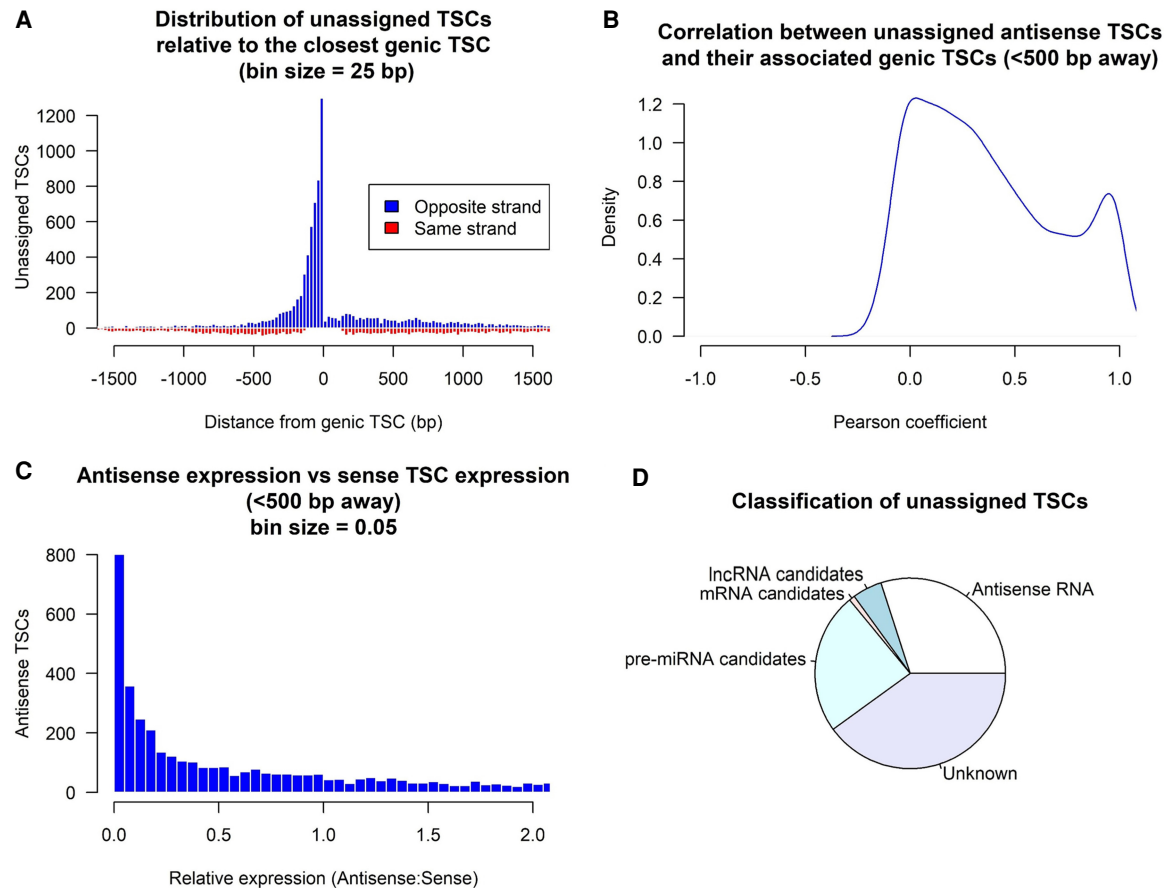


**Figure 4.** Identification of unassigned TSCs through bioinformatic approaches. (A) Distance between unassigned TSCs and their nearest genic TSCs. A high number of elements localized within 500 bp upstream of genic TSCs but on the opposite strand. (B) Correlation of expression from antisense TSCs (CPM > 3) with expression from sense TSCs. (C) Expression of the antisense variant (CPM > 3) relative to the sense variant. (D) Putative roles attributed to unassigned TSCs.

predicted their coding potential based on *k*-mer frequencies, codon usage, and open reading frame (ORF) coverage. As a result, we identified 2306 TSCs associated with potential lncRNAs (Supplemental File S2) and 259 TSCs associated with potential mRNAs (Supplemental File S3). Lastly, we predicted pre-miRNA structures among the remaining models and identified 11,266 TSCs for candidate miRNA genes (Supplemental File S4), which is slightly over the estimated number of human miRNA candidates (Alles et al. 2019). After identifying TSCs for potential mRNAs, lncRNAs, and pre-miRNAs, the number of remaining unassigned elements decreased to 18,259. The epigenetic marks at these loci showed unclear patterns (Supplemental Fig. S6), and the RAMPAGE signal failed to cluster samples by tissue except for a few cases (Supplemental Fig. S7), suggesting the remaining TSCs represented technical artifacts. However, we could not discard the possibility that these TSCs corresponded to unannotated small RNAs, other types of RNAs, or repetitive elements.

#### Analysis of promoter activity and specificity

As RAMPAGE relies on the quantification of 5' signal from mature transcripts, this technique also provides useful information for gene expression and promoter activity studies. To show this aspect, we first analyzed our samples by hierarchical clustering

(Fig. 5A). Samples grouped according to tissue and higher-order structures, proving that the method was quantitative enough to separate samples appropriately. All the RAMPAGE information, including peak location, gene assignment, quality of the gene assignment, peak status by epigenetic signal, and other features, as well as the number of tags in each sample, was implemented into a TSC atlas (Supplemental Table S2). Genic TSCs are also available as GTF file (Supplemental File S5). To evaluate the complexity of the data set and to identify groups of potentially coregulated elements, we generated a coexpression network based on the number of RAMPAGE tags in each sample (Fig. 5B). The resulting network comprised 34 modules of coexpressed TSCs with different degrees of tissue specificity, which varied from single tissues, such as trachea or thymus, to high-level structures, such as brain or digestive epithelium (Fig. 5C; Supplemental Table S3). The largest module was highly correlated to testis and comprised 6854 TSCs, followed by the brain module with 3194 TSCs and the intestines module with 1888 TSCs. These numbers were consistent with studies in human and mouse, which have shown that the testis expresses the largest number of tissue-specific genes (over twice as many as the second-ranked tissue, the brain cortex) (Guo et al. 2005; Djureinovic et al. 2014). Promoters from each module were significantly enriched in binding motifs for transcription factors associated with their respective tissues (Supplemental Fig. S8). For

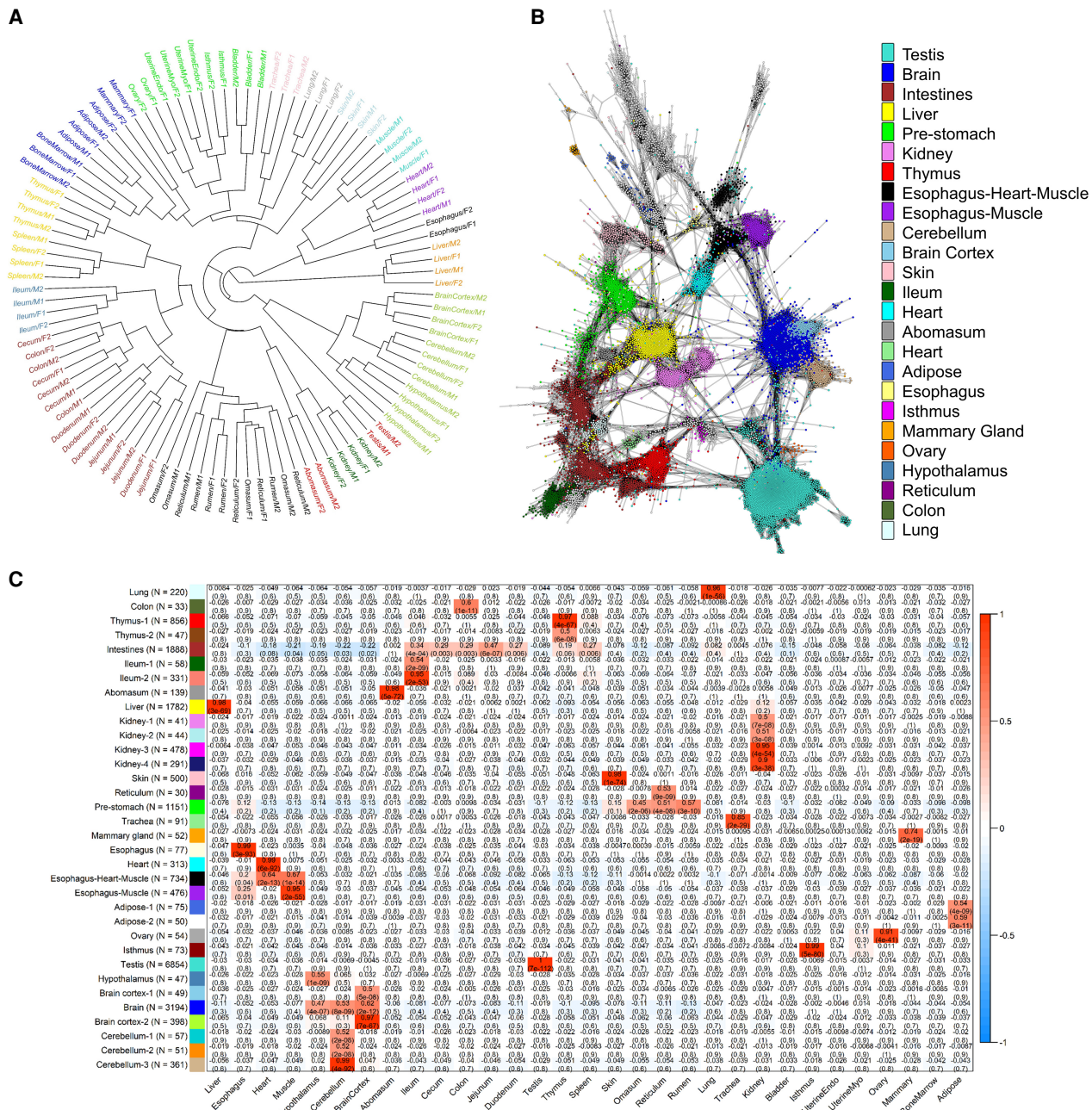


**Figure 5.** Promoter activity detected in 31 cattle tissues by RAMPAGE. (A) Sample dendrogram based on RAMPAGE signal. Samples grouped according to tissue, system, and higher-order structures. (B) TSC-to-TSC network generated based on Pearson's correlations. This network shows the diversity of tissue-specific promoters in our data set. Figure was generated using a minimum correlation of 0.75 in the Graphia v2.0 software (Freeman et al. 2020). (C) Modules of coexpressed TSCs indicating Pearson's correlations to each tissue and P-values. To validate the RAMPAGE signal from a quantitative perspective, we compared RAMPAGE counts to conventional RNA-seq gene counts in seven tissues from the same two male individuals. Estimates of gene expression by RAMPAGE were highly reproducible between biological replicates (average Pearson's  $R=0.94$ ,  $SD=0.03$ ) (Supplemental Table S4, Supplemental Fig. S9), consistent with the reproducibility of conventional RNA-seq (average Pearson's  $R=0.98$ ,  $SD=0.01$ ) (Supplemental Fig. S10). Absolute quantification of gene expression was comparable between the two techniques (average Pearson's  $R=0.76$ ,  $SD=0.03$ ) (Supplemental Figs. S11, S12), and detection of differentially expressed genes was strongly correlated between RNA-seq and RAMPAGE (average Pearson's  $R=0.9$ ,  $SD=0.05$ ) (Supplemental Fig. S13). Overall, these results suggest slight differences in global transcriptome measurement by RAMPAGE and RNA-seq, although both assays captured highly similar levels of differential gene expression.

instance, the esophagus-heart-muscle module was enriched in binding motifs for all members of the myocyte enhancer factor 2 (MEF2) family, which are known to regulate muscle-specific genes and muscle development (Gossett et al. 1989).

After evaluating data set complexity and validating the quantitative aspects of our data, we proceeded to evaluate the use of alternative promoters across tissues and the composition of each network module. Expression profiles from alternative TSCs of



the same gene across the data set were generally independent, as evidenced by the low correlation coefficients obtained in pairwise comparisons (Fig. 6A). This observation suggested that most of the alternative TSCs were regulated by different biological mechanisms. Most of the TSCs were expressed in only one or a few tissues, with about 6000 ubiquitous TSCs (Fig. 6B). It is worth mentioning that some tissues, such as that of the lung and trachea, expressed even more genes than the testis and brain but showed few tissue-specific TSCs in comparison (Fig. 5C). To evaluate the expression of genes from tissue-specific TSCs, we analyzed expression from 3336 genes detected in at least two coexpression modules. We found 601 genes whose transcripts originated from alternative promoters in either testis or brain, which represented the highest use of alternative promoters between modules (Fig. 6C–E). The GO analysis of genes shared by testis and brain revealed a significant enrichment in terms related to cytoskeleton components, mi-

crothubule binding, ATP-binding kinase activity, synapse, cell–cell adhesion, microtubule-based movement and transport, and kinesin activity (Supplemental Table S5). We also found statistical enrichment in synapse pathways, including GABAergic synapse, cholinergic synapse, glutamatergic synapse, and serotonergic synapse, as well as critical pathways from the hypothalamus–pituitary–gonad (HPG) axis, such as GnRH and GABA signaling. The high number of members and use of alternative promoters found in these two tissues evidenced the complexity they acquired throughout evolution. Following the testis–brain combination, we found testis–intestines, with 357 genes, and testis–liver, with 325 genes, using alternative promoters in each tissue. Genes shared by testis and intestines were highly enriched in GO terms related to cell cycle and division control, GTPase activity regulation, kinase activity, and additional groups of processes with lower enrichment (Supplemental Table S5). Genes shared by testis and

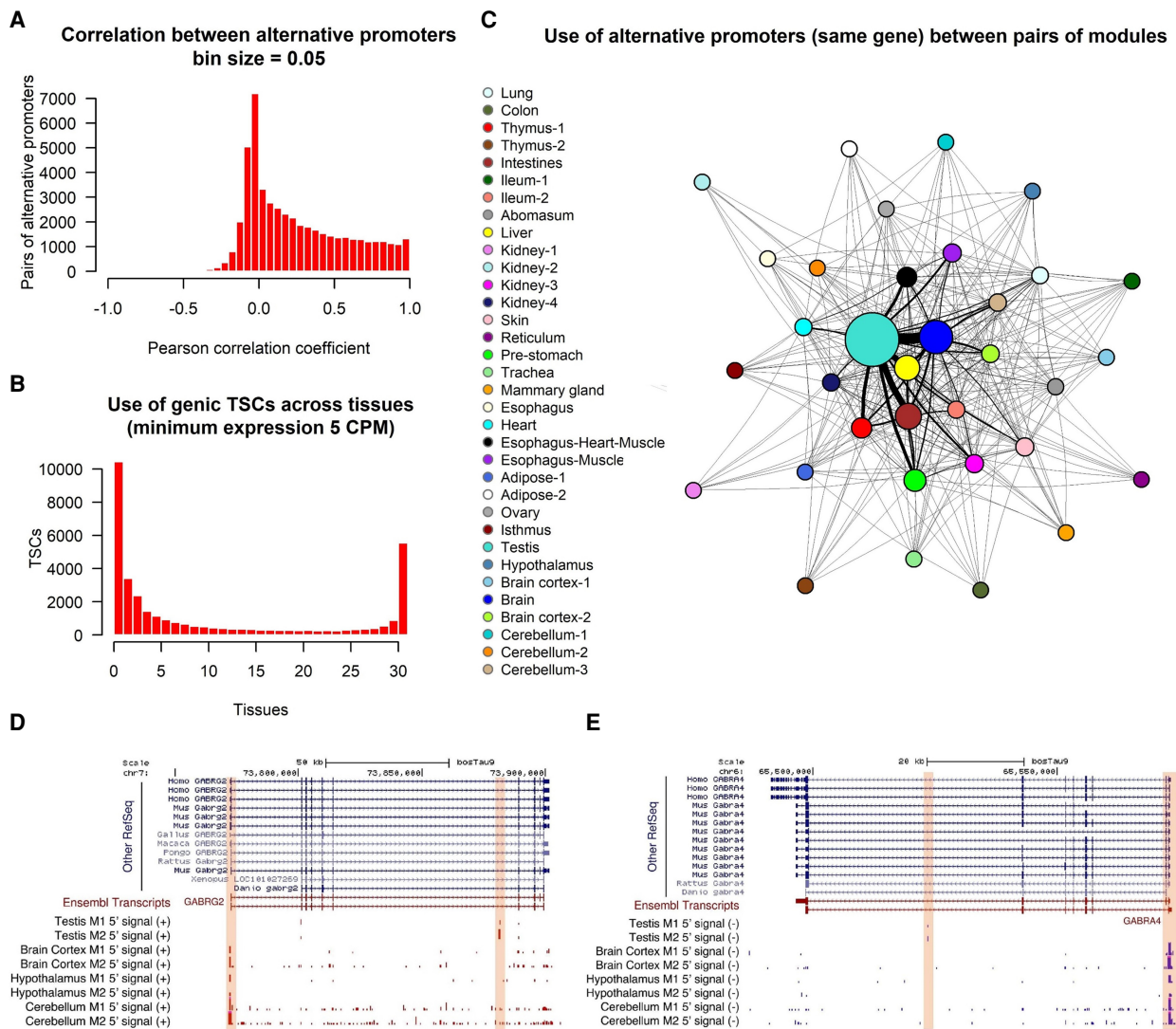


**Figure 6.** Usage of promoters across bovine tissues. (A) Correlation between pairs of alternative TSCs from the same gene (>5 CPM). Alternative TSCs were generally independent from each other. (B) Usage of TSCs across tissues. Most of the TSCs were expressed in only one or a few tissues, whereas about 6000 TSCs were ubiquitously expressed. (C) Use of alternative TSCs between pairs of tissues. Sphere size represents the number of TSC members in the module, and edge thickness represents the number of common genes expressed from alternative (tissue-specific) TSCs. (D,E) Examples of tissue-specific promoters in brain and testis. The *GABRG2* and *GABRA1* genes are members of the GABAergic synapse pathway.

liver, on the other hand, were slightly enriched in terms related to acyl-CoA-binding, mitochondrial components, and steroid and lipid metabolism (Supplemental Table S5).

## Discussion

In this study, we analyzed a large collection of bovine tissues from both sexes using the RAMPAGE approach, identifying thousands of TSCs associated with protein-coding and lncRNA genes. The diversity of analyzed tissues captured the expression of 18,312 previously annotated genes. However, no expression was detected for 5016 genes, likely reflecting the absence of embryonic/fetal developmental genes in our collection of tissues from juvenile/adult animals. Thus, an additional analysis of samples at different stages of development should be performed to generate an even more comprehensive TSS annotation of the bovine genome. It is worth mentioning that samples from this study belonged to the same closed, inbred herd as the Line 1 reference cow. The genetic proximity between our samples and the reference genome likely contributed to the high mapping rates, whereas the low genetic variation provided by the inbred background of Line 1 likely contributed to the high correlations between samples.

Our data set allowed us to identify several known and novel TSCs with a broad range of sizes. Size variation was expected as mammalian promoters are known to allow transcription to start from both well-defined positions (TATA-box-enriched promoters) and broad intervals (CpG-rich promoters) (Carninci et al. 2006). In fact, we found that regions upstream of narrow TSCs were enriched with TATA-box elements, whereas regions upstream of broad TSCs were enriched in GC-box and CCAAT-box elements. In addition, novel TSCs were supported by experimental evidence that revealed the presence of chromatin accessibility and transcriptional activation marks (H3K4me3, H3K27ac) and near absence of H3K4me1, an epigenetic mark historically used for enhancer annotation (Heintzman et al. 2007), which implicated these novel TSCs as part of promoters. In addition to TSCs associated with annotated genes, we found many unassigned TSCs that supported the existence of pervasive transcription. A considerable number of unassigned TSCs were upstream of genic TSCs and seemed to be a consequence of bidirectional promoter activity. As shown in mouse (Lepoivre et al. 2013), transcripts from bidirectional promoters were more correlated to each other than transcripts from alternative TSCs of the same gene, suggesting a common regulatory mechanism. Furthermore, antisense transcripts presented low expression levels in comparison to their complementary sense transcripts, supporting the concept of pervasive transcription by erratic behavior of the polymerase.

Even though the RAMPAGE method has important advantages over other 5'-seq techniques for TSC identification (Adiconis et al. 2018), including CAGE (Takahashi et al. 2012) due to extensive use of paired-end information, false TSCs were expected to arise as products of incomplete cDNA synthesis and mRNA degradation. We estimated that ~30% of the 13,209 novel TSCs in annotated exons could be false positives as shown by the low H3K4me3 signal. These elements could have been caused by recapping, which has been reported in RNAs with truncated 5'-ends (Otsuka et al. 2009) and within the body of mRNAs (Affymetrix/Cold Spring Harbor Laboratory ENCODE Transcriptome Project 2009). However, due to the low number of tissues with epigenetic information in comparison to the RAMPAGE data set, our evidence was insufficient to identify and discard all potential artifacts. A global estimation based on the assumptions that artifacts are

most frequent in exons (downstream from the strongest TSC), expressed to a lower extent (<25%), and correlated to the strongest TSC for being part of the same transcript (Pearson's  $R > 0.5$ ) suggested that 4059 (8.7%) of the genic TSCs could be false. This estimation supported our initial estimation by epigenetic signal in the reduced validation data set. However, the identification of these sites needs to be corroborated by additional epigenetic information from other tissues.

The analysis of coexpression networks revealed a high number of genes expressed in both brain and testicle under different tissue-specific TSCs. The high similarity between brain and testis expression profiles was reported years ago in mouse and human (Guo et al. 2003, 2005). The mechanisms and epigenetic factors contributing to the projection of the brain expression program on the testis are unclear, although intriguing. It has been proposed that the HPG could be implicated in the maintenance of this similarity, given the importance of the brain expression program for human speciation and transmission to the offspring (Guo et al. 2005). Our study, however, showed that although brain and testis share a high number of genes, transcripts are expressed from tissue-specific promoters. These promoters could be generating isoforms with different and unique functions. This information could be valuable to understand the regulatory mechanisms operating behind tissue-specific expression profiles.

With our set of new TSCs, the bovine ratio of TSS to genes reached a level comparable to the human and mouse genomes. Hopefully, this annotation will improve our understanding of the genetic control of complex livestock traits, complementing studies from other members of the FAANG community. In addition, our data will improve the connection between genotypes and phenotypes to exploit predictive models in the breeding field, provide new biological explanations for genetic diseases reportedly unexplained based on other annotations, and contribute to the study of genome evolution through comparative studies with other species.

## Methods

### Sample collection

Samples from abomasum, adipose, bladder, brain cortex, bone marrow, cecum, cerebellum, colon, duodenum, esophagus, heart, hypothalamus, ileum, isthmus, jejunum, kidney, liver, lung, skeletal muscle, mammary gland, omasum, ovary, reticulum, rumen, skin, spleen, testis, thymus, trachea, uterine endometrium, and uterine myometrium were collected from two female and two male 14-mo-old Line 1 Herefords provided by the Fort Keogh Livestock and Range Research Laboratory. Samples belonged to the same closed, inbred herd as the original Line 1 reference cow.

Sample collection was performed with all the necessary permissions, following Protocol for Animal Care and Use 18464, approved by the Institutional Animal Care and Use Committee (IACUC), University of California, Davis. Cattle were slaughtered by captive bolt under USDA inspection at the University of California, Davis, and samples were collected within 1 h post euthanasia. Collected tissue samples were flash-frozen in liquid nitrogen and stored at  $-80^{\circ}\text{C}$  until processing.

### RAMPAGE library preparation

Frozen tissues kept at  $-80^{\circ}\text{C}$  were homogenized with a mortar and pestle in liquid nitrogen. Total RNA was extracted using TRIzol (Invitrogen) followed by a column clean-up using the Direct-zol RNA mini prep plus kit (Zymo Research) and performing an

in-column DNA digestion. Integrity of the DNase-treated RNA was verified on the Experion electrophoresis system (Bio-Rad). The RNA quality indicator (RQI) varied from 7.5 to 9.7, indicating good-quality RNA, excepting liver from male A, which had a borderline RQI of 6.9.

Following the method described by Batut and Gingeras (2013), DNase-treated RNA was subjected to terminator digestion (TEX enzyme, Epicentre) to degrade 5'-monophosphate RNA (16S and 18S ribosomal RNA). Random primers bearing an adapter sequence overhang were annealed to the RNA, which was then subjected to RT, leaving a string of terminal cytosines. Template-switching oligonucleotides (TSOs) containing the library identification barcodes were then hybridized to these terminal cytosines, prompting the reverse transcriptase to switch templates and add the TSO sequence to the end of the newly synthesized cDNA. The TSO bears an Illumina adaptor sequence, such that only 5'-complete cDNAs are amplifiable, whereas non-5'-complete molecules are not. Libraries were then quantified by qPCR to pool multiple samples for sequencing.

Libraries were pooled in equimolar amounts, and 5' caps were oxidized with sodium periodate. To prepare for cap trapping, 5' caps were biotinylated, and RNA molecules were pulled down using streptavidin magnetic beads. Finally, pooled libraries were PCR-amplified and size-selected using AmPure XP magnetic beads. Final pooled libraries were quantified in the NanoDrop spectrophotometer (Thermo Fisher Scientific) and the Bioanalyzer 2100 high-sensitivity DNA chip (Agilent Technologies). Libraries had the expected size range of 300–1000 bp and were sequenced on an Illumina HiSeq 4000 system, generating paired-end reads of either 100 or 150 bp.

### RNA-seq data analysis

Data for RNA-seq (Kern et al. 2018) were downloaded from the NCBI Gene Expression Omnibus (GEO; <https://www.ncbi.nlm.nih.gov/geo/>) (accession number GSE158430). Reads were trimmed using Trimmomatic (v0.33) to remove Illumina sequencing adapters and low-quality bases. Settings for adapter removal included a maximum of two mismatches, a palindrome clip threshold of 30, and a simple clip threshold of 10. Leading and trailing bases of quality less than three were removed. Sliding window trimming was conducted using a window size of four and minimum average quality of 15. After processing, reads <36 bp were discarded. Samples were aligned to the ARS-UCD1.2 *Bos taurus* reference genome using STAR v2.6.1 (Dobin et al. 2013) with options `--outFilterScoreMinOverRead 0.85` and `--seedSearchStartLmax 30`.

### RAMPAGE data analysis

Samples were aligned to the ARS-UCD1.2 *B. taurus* reference genome using STAR in two-pass mode. The first 6 nt of the first read (barcodes) were removed before alignment as part of the demultiplexing step. The last 15 nt of the second read corresponded to the RT primer; thus, they were soft-clipped using the `--clip5pNbases` option during the alignment step. Only uniquely mapped reads were kept for subsequent analyses. To improve the specificity of the peak calling and the accuracy of transcript quantification, duplicates were marked and removed based on the alignment coordinates and the last 15 nt of the second read (random primer), which were used as a pseudorandom single-molecule barcode to distinguish true duplicates. Alignments from the same sample were merged before peak calls. A preliminary assessment of data quality was performed using hierarchical clustering of gene counts generated by featureCounts v1.6.2 (Liao et al. 2014)

before peak calling. Samples showing anomalous expression profiles compared with other biological replicates from the same tissue were discarded from subsequent analyses.

### RAMPAGE peak calling

The 5' coordinate of each cDNA was recorded and compiled into a single wiggle file as a quantification of every possible TSS in the data set. Then, the same was performed for every genomic position covered by downstream reads to create a signal background for the peak calling algorithm. Peak calling was conducted using the Python script developed by Batut et al. (2013) with a dispersion parameter of four, a background weight of 0.6, and an FDR of  $1 \times 10^{-8}$  in the combined data set (Supplemental Code S1). Briefly, the algorithm works as a sliding window that, for each position in the genome, assesses the statistical enrichment of 5' signal against a negative binomial background distribution. The coverage by downstream reads in such window is used to subtract a pseudo-count from the 5' signal so that significance is harder to achieve at highly transcribed exon positions. Then, neighboring windows are merged and trimmed at the edges down to the first base with signal.

To increase the sensitivity for tissue-specific peaks, each tissue was also analyzed separately using a dispersion parameter of 0.2, a background weight of 0.8, and an FDR of  $1 \times 10^{-8}$ . Tissue-specific TSCs undetected in the combined data set, supported by at least three independent RAMPAGE tags, located outside exons, and conserved in at least two biological replicates, were incorporated into the global list of TSCs.

### Gene assignment

TSCs were assigned to genes using featureCounts in stranded mode (`-s 1`) and the Ensembl v95 annotation. Gene associations supported by fewer than three independent fragments were considered weak associations. To exclude spurious associations generated by run-off transcription, namely, transcription that failed to terminate at the right site and continued over a downstream gene, associations to alternative genes supported by fivefold fewer reads than the most supported gene were disregarded. For quantification purposes, the RAMPAGE signal was normalized by library size (total number of reads associated with TSCs). Genes were considered as expressed when their expression (normalized with respect to all the RAMPAGE tags assigned to genes) reached a minimum of 3 CPM.

### Expression quantification by RNA-seq and RAMPAGE

For comparison between RAMPAGE and RNA-seq, RAMPAGE gene expression was quantified using the number of 5' tags in TSCs attributed to each gene. Genes with fewer than 10 total counts across all samples were removed from the analysis before normalization by DESeq2 (Love et al. 2014) to eliminate background noise. Normalized counts were log-transformed and used to calculate Pearson's correlations between biological replicates for each tissue. Log-transformed normalized counts from all tissues were then pooled to calculate the overall Pearson's correlations between male replicates in all tissues and female replicates in all tissues. Gene expression was evaluated from RNA-seq data for a subset of seven tissues. Raw expression values for genes in the *B. taurus* annotation (Ensembl v95) were calculated from uniquely mapped reads using the SummarizeOverlaps function from the GenomicAlignments R package (Lawrence et al. 2013) with the "union," paired-end, and stranded options. Genes with fewer than 10 total counts across all samples were removed from the analysis before normalization to eliminate background noise.

Gene counts were then normalized by DESeq2 and log-transformed. Log-transformed normalized counts from all seven tissues were pooled to calculate the overall Pearson's correlation between male replicates. For the seven tissues for which RNA-seq data were available, log-transformed normalized counts were used to calculate Pearson's correlations between RNA-seq and RAMPAGE. Finally, differential gene expression was compared between RNA-seq and RAMPAGE. From RNA-seq counts, differentially expressed genes (DEGs) were identified for each pair of tissues using DESeq2 and lfcShrink (type="apeglm," lfcThreshold = 1), given an *s*-value < 0.005. The log fold change (logFC) of these DEGs was then calculated by DESeq2 according to RNA-seq and RAMPAGE signal and used to calculate Pearson's correlations.

### ATAC-seq and ChIP-seq data analysis

ChIP-seq and ATAC-seq data (Kern et al. 2018) were downloaded from the NCBI Gene Expression Omnibus (GEO; <https://www.ncbi.nlm.nih.gov/geo/>) (accession number GSE158430). ATAC-seq reads were trimmed with Trim Galore! v0.4.0 (-q 20 -a CTGTCTCTTATA -stringency 1 -length 10) (<https://github.com/FelixKrueger/TrimGalore>) and aligned to the ARS-UCD1.2 genome with BWA-MEM (Li and Durbin 2009). Duplicate alignments were removed using Picard Tools v2.9.1 (<https://broadinstitute.github.io/picard/>). Low-quality alignments (*q* < 15) were removed with SAMtools v1.9 (Li et al. 2009). ChIP-seq reads were processed following the method of the original study (Kern et al. 2018). To visualize signal, the bamCoverage function of the deepTools v3.2.0 software (Ramírez et al. 2016) was used to calculate normalized coverage (CPM) in 10-bp windows genome-wide. For ChIP-seq, signal from input libraries was first subtracted with deepTools bigwigCompare. Normalized signal from ATAC-seq and ChIP-seq libraries was plotted alongside RAMPAGE 5' signal on the UCSC Genome Browser. The deepTools computeMatrix and plotHeatmap functions were also used to plot normalized epigenetic signal at TSCs, plotting the median signal above heatmaps and using the interpolation method "bilinear" for smoothing. The average epigenetic signal (CPM) at TSCs was calculated with the bigWigAverageOverBed function from the UCSC Genome Browser utilities.

### Identification of binding motifs

The abundance of TATA-, GC-, and CCAAT-boxes in regions 200 bp upstream of to 200 bp downstream from novel TSCs was visualized using the seqPattern R package (<https://bioconductor.org/packages/release/bioc/html/seqPattern.html>). The search was performed using the TATA-box binding protein (TBP) model included in the package, the MA0079.2.pfm JASPAR model for Sp1 transcription factor (SP1), and the MA0060.3.pfm JASPAR model for nuclear transcription factor Y (NFYA).

Statistical enrichment was evaluated using the "findMotifsGenome.pl" tool from HOMER v4.10.4 (Heinz et al. 2010). Background consisted of either random sequences from the rest of the genome or sequences from the rest of the gene body depending on the location of the TSC evaluated (promoters and intergenic regions, or exons and introns, respectively). The search was conducted on sequences 300 bp upstream of to 100 bp downstream from the TSCs using binding motifs for TBP, SP1, and NFYA available in the HOMER database.

### Attribution of unassigned TSCs

Unguided partial transcript models were generated for RNAs derived from unassigned TSCs using StringTie v2.0.4 (Pertea et al. 2015) in --fr stranded mode, a minimum isoform fraction of

zero, a minimum assembled transcript length of 30, a minimum of one read per base pair coverage, and trimming based on coverage disabled. Antisense RNAs mapping to the gene body were identified using featureCounts in the opposite stranded mode (-s 2). Putative protein-coding and lncRNA genes were predicted based on *k*-mer frequency, codon use, and ORF coverage using the FEELnc software (Wucher et al. 2017). Lastly, prediction of pre-miRNA candidates was performed using the miRNAfold tool (Tav et al. 2016) with a sliding window size of 60 bp and FASTA files containing the remaining partial transcripts as input.

### Evaluation of alternative promoter usage

Correlations between alternative TSCs from the same gene were evaluated considering highly expressed genic TSCs (>5 CPM normalized with respect to the number of RAMPAGE tags assigned to genic TSCs) through the Pearson correlation coefficient.

The use of alternative promoters was analyzed through signed coexpression networks generated by the WGCNA R package (Langfelder and Horvath 2008). To reduce noise, networks were constructed for TSCs with a minimum expression of 3 CPM in at least two samples of any tissue. The adjacency matrix was generated using variance-stabilized counts as input, biweight midcorrelations, and a soft-thresholding power of 12. Modules were determined using the dynamic hybrid tree cut algorithm with a sensitivity (deepSplit) of two and PAM mode activated.

### GO analysis

Functional annotation clustering was conducted using official gene symbols in DAVID bioinformatics v6.8 (Huang et al. 2009). We used the *Homo sapiens* model as background due to its more comprehensive pathway annotation. The analysis was performed using the default categories (OMIM\_DISEASE, COG\_ONTOLOGY, UP\_KEYWORDS, UP\_SEQ\_FEATURE, GOTERM\_BP\_DIRECT, GOTERM\_CC\_DIRECT, GOTERM\_MF\_DIRECT, BBID, BIOCARTA, KEGG\_PATHWAY, INTERPRO, PIR\_SUPER\_FAMILY, SMART) and medium stringency.

### Data access

All raw sequencing data generated in this study have been submitted to the NCBI BioProject database (<https://www.ncbi.nlm.nih.gov/bioproject/>) under accession number PRJNA630504. As samples were submitted using their FAANG nomenclature, sample M1 is found as M08, sample M2 is found as M22, sample F1 is found as F05, and sample F2 is found as F12. The Python script used to identify RAMPAGE peaks is available as Supplemental Material (Supplemental Code S1). Additionally, we generated a GTF file with partial transcripts (Supplemental File S1), a BED file with TSCs associated with lncRNAs (Supplemental File S2), a BED file with TSCs associated with unannotated genes (Supplemental File S3), a BED file with TSCs associated with pre-miRNAs (Supplemental File S4), and a GTF file with genic TSC annotations (Supplemental File S5).

### Competing interest statement

The authors declare no competing interests.

### Acknowledgments

Funding for this project was provided by the U.S. Department of Agriculture, National Institute of Food and Agriculture, Agriculture and Food Research Initiative (USDA-NIFA-AFRI) grant no. 2017-67015-26297 to P.J.R. ChIP-seq data were generated as

part of USDA-NIFA-AFRI grant no. 2015-43567015-22940 to H.Z. and P.J.R. M.M.H. was supported by a USDA-NIFA National Needs Fellowship grant (USDA-NIFA Competitive Grant Project no. 2014-38420-21796) and an Austin Eugene Lyons Fellowship.

## References

- Abugessaisa I, Noguchi S, Hasegawa A, Kondo A, Kawaji H, Carninci P, Kasukawa T. 2019. refTSS: a reference data set for human and mouse transcription start sites. *J Mol Biol* **431**: 2407–2422. doi:10.1016/j.jmb.2019.04.045
- Adiconis X, Haber AL, Simmons SK, Levy Moonshine A, Ji Z, Busby MA, Shi X, Jacques J, Lancaster MA, Pan JQ, et al. 2018. Comprehensive comparative analysis of 5'-end RNA-sequencing methods. *Nat Methods* **15**: 505–511. doi:10.1038/s41592-018-0014-2
- Affymetrix/Cold Spring Harbor Laboratory ENCODE Transcriptome Project. 2009. Post-transcriptional processing generates a diversity of 5'-modified long and short RNAs. *Nature* **457**: 1028–1032. doi:10.1038/nature07759
- Alles J, Fehlmann T, Fischer U, Backes C, Galata V, Minet M, Hart M, Abulhalima M, Grässer FA, Lenhof H-P, et al. 2019. An estimate of the total number of true human miRNAs. *Nucleic Acids Res* **47**: 3353–3364. doi:10.1093/nar/gkz097
- Batut P, Gingeras TR. 2013. RAMPAGE: promoter activity profiling by paired-end sequencing of 5'-complete cDNAs. *Curr Protoc Mol Biol* **104**: Unit-25B.11. doi:10.1002/0471142727.mb25b11s104
- Batut P, Dobin A, Plessy C, Carninci P, Gingeras TR. 2013. High-fidelity promoter profiling reveals widespread alternative promoter usage and transposon-driven developmental gene expression. *Genome Res* **23**: 169–180. doi:10.1101/gr.139618.112
- Bevacqua RJ, Fernandez-Martín R, Savy V, Canel NG, Gismondi MI, Kues WA, Carlson DF, Fahrner SC, Niemann H, Taboga OA, et al. 2016. Efficient edition of the bovine PRNP prion gene in somatic cells and IVF embryos using the CRISPR/Cas9 system. *Theriogenology* **86**: 1886–1896.e1. doi:10.1016/j.theriogenology.2016.06.010
- The Bovine Genome Sequencing and Analysis Consortium, Elsik CG, Tellam RL, Worley KC. 2009. The genome sequence of taurine cattle: a window to ruminant biology and evolution. *Science* **324**: 522–528. doi:10.1126/science.1169588
- Britt JH, Cushman RA, Dechow CD, Dobson H, Humblot P, Hutjens MF, Jones GA, Ruegg PS, Sheldon IM, Stevenson JS. 2018. Invited review: learning from the future—a vision for dairy farms and cows in 2067. *J Dairy Sci* **101**: 3722–3741. doi:10.3168/jds.2017-14025
- Carninci P, Sandelin A, Lenhard B, Katayama S, Shimokawa K, Ponjavic J, Semple CAM, Taylor MS, Engström PG, Frith MC, et al. 2006. Genome-wide analysis of mammalian promoter architecture and evolution. *Nat Genet* **38**: 626–635. doi:10.1038/ng1789
- Djreinovic D, Fagerberg L, Hallström B, Danielsson A, Lindskog C, Uhlén M, Pontén F. 2014. The human testis-specific proteome defined by transcriptomics and antibody-based profiling. *Mol Hum Reprod* **20**: 476–488. doi:10.1093/molehr/gau018
- Dobin A, Davis CA, Schlesinger F, Drenkow J, Zaleski C, Jha S, Batut P, Chaisson M, Gingeras TR. 2013. STAR: ultrafast universal RNA-seq aligner. *Bioinformatics* **29**: 15–21. doi:10.1093/bioinformatics/bts635
- Engström PG, Suzuki H, Ninomiya N, Akalin A, Sessa L, Lavorgna G, Brozzi A, Luzzi L, Tan SL, Yang L, et al. 2006. Complex loci in human and mouse genomes. *PLoS Genet* **2**: e47. doi:10.1371/journal.pgen.0020047
- Ernst J, Kellis M. 2017. Chromatin-state discovery and genome annotation with ChromHMM. *Nat Protoc* **12**: 2478–2492. doi:10.1038/nprot.2017.124
- The FAANG Consortium, Andersson L, Archibald AL, Bottema CD, Brauning R, Burgess SC, Burt DW, Casas E, Cheng HH, Clarke L, et al. 2015. Coordinated international action to accelerate genome-to-phenome with FAANG, the functional annotation of animal genomes project. *Genome Biol* **16**: 57. doi:10.1186/s13059-015-0622-4
- The FANTOM Consortium and the RIKEN PMI and CLST (DGT). 2014. A promoter-level mammalian expression atlas. *Nature* **507**: 462–470. doi:10.1038/nature13182
- Freeman TC, Horsewell S, Patir A, Harling-Lee J, Regan T, Shih BB, Prendergast J, Hume DA, Angus T. 2020. Graphia: a platform for the graph-based visualisation and analysis of complex data. bioRxiv doi:10.1101/2020.09.02.279349
- Gossett LA, Kelvin DJ, Sternberg EA, Olson EN. 1989. A new myocyte-specific enhancer-binding factor that recognizes a conserved element associated with multiple muscle-specific genes. *Mol Cell Biol* **9**: 5022–5033. doi:10.1128/MCB.9.11.5022
- Guo J, Zhu P, Wu C, Yu L, Zhao S, Gu X. 2003. In silico analysis indicates a similar gene expression pattern between human brain and testis. *Cytogenet Genome Res* **103**: 58–62. doi:10.1159/000076290
- Guo JH, Huang Q, Studholme DJ, Wu CQ, Zhao Z. 2005. Transcriptomic analyses support the similarity of gene expression between brain and testis in human as well as mouse. *Cytogenet Genome Res* **111**: 107–109. doi:10.1159/000086378
- Heintzman ND, Stuart RK, Hon G, Fu Y, Ching CW, Hawkins RD, Barrera LO, Van Calcar S, Qu C, Ching KA, et al. 2007. Distinct and predictive chromatin signatures of transcriptional promoters and enhancers in the human genome. *Nat Genet* **39**: 311–318. doi:10.1038/ng1966
- Heinz S, Benner C, Spann N, Bertolino E, Lin YC, Laslo P, Cheng JX, Murre C, Singh H, Glass CK. 2010. Simple combinations of lineage-determining transcription factors prime cis-regulatory elements required for macrophage and B cell identities. *Mol Cell* **38**: 576–589. doi:10.1016/j.molcel.2010.05.004
- Huang DW, Sherman BT, Lempicki RA. 2009. Systematic and integrative analysis of large gene lists using DAVID bioinformatics resources. *Nat Protoc* **4**: 44–57. doi:10.1038/nprot.2008.211
- Ju Z, Jiang Q, Wang J, Wang X, Yang C, Sun Y, Zhang Y, Wang C, Gao Y, Wei X, et al. 2020. Genome-wide methylation and transcriptome of blood neutrophils reveal the roles of DNA methylation in affecting transcription of protein-coding genes and miRNAs in *E. coli*-infected mastitis cows. *BMC Genomics* **21**: 102. doi:10.1186/s12864-020-6526-z
- Kern C, Wang Y, Chitwood J, Korf I, Delany M, Cheng H, Medrano JF, Van Eenennaam AL, Ernst C, Ross P, et al. 2018. Genome-wide identification of tissue-specific long non-coding RNA in three farm animal species. *BMC Genomics* **19**: 684. doi:10.1186/s12864-018-5037-7
- Kodzius R, Kojima M, Nishiyori H, Nakamura M, Fukuda S, Tagami M, Sasaki D, Imamura K, Kai C, Harbers M, et al. 2006. CAGE: cap analysis of gene expression. *Nat Methods* **3**: 211–222. doi:10.1038/nmeth0306-211
- Langfelder P, Horvath S. 2008. WGCNA: an R package for weighted correlation network analysis. *BMC Bioinformatics* **9**: 559. doi:10.1186/1471-2105-9-559
- Lawrence M, Huber W, Pagès H, Aboyoun P, Carlson M, Gentleman R, Morgan MT, Carey VJ. 2013. Software for computing and annotating genomic ranges. *PLoS Comput Biol* **9**: e1003118. doi:10.1371/journal.pcbi.1003118
- Lepoivre C, Belhocine M, Bergon A, Griffon A, Yammine M, Vanhille L, Zacarias-Cabeza J, Garibal M-A, Koch F, Maqbool M, et al. 2013. Divergent transcription is associated with promoters of transcriptional regulators. *BMC Genomics* **14**: 914. doi:10.1186/1471-2164-14-914
- Li H, Durbin R. 2009. Fast and accurate short read alignment with Burrows-Wheeler transform. *Bioinformatics* **25**: 1754–1760. doi:10.1093/bioinformatics/btp324
- Li H, Handsaker B, Wysoker A, Fennell T, Ruan J, Homer N, Marth G, Abecasis G, Durbin R, 1000 Genome Project Data Processing Subgroup. 2009. The Sequence Alignment/Map format and SAMtools. *Bioinformatics* **25**: 2078–2079. doi:10.1093/bioinformatics/btp352
- Liao Y, Smyth GK, Shi W. 2014. featureCounts: an efficient general purpose program for assigning sequence reads to genomic features. *Bioinformatics* **30**: 923–930. doi:10.1093/bioinformatics/btt656
- Love MI, Huber W, Anders S. 2014. Moderated estimation of fold change and dispersion for RNA-seq data with DESeq2. *Genome Biol* **15**: 550. doi:10.1186/s13059-014-0550-8
- Meers MP, Adelman K, Duronio RJ, Strahl BD, McKay DJ, Matera AG. 2018. Transcription start site profiling uncovers divergent transcription and enhancer-associated RNAs in *Drosophila melanogaster*. *BMC Genomics* **19**: 157. doi:10.1186/s12864-018-4510-7
- Null D, VanRaden PM, Rosen B, O'Connell J, Bickhart D. 2019. Using the ARS-UCD1.2 reference genome in U.S. evaluations. *Interbull Bulletin* **30**: 30–34.
- Otsuka Y, Kedersha NL, Schoenberg DR. 2009. Identification of a cytoplasmic complex that adds a cap onto 5'-monophosphate RNA. *Mol Cell Biol* **29**: 2155–2167. doi:10.1128/MCB.01325-08
- Perteau M, Perteau GM, Antonescu CM, Chang T-C, Mendell JT, Salzberg SL. 2015. StringTie enables improved reconstruction of a transcriptome from RNA-seq reads. *Nat Biotechnol* **33**: 290–295. doi:10.1038/nbt.3122
- Ramírez F, Ryan DP, Grünig B, Bhardwaj V, Kilpert F, Richter AS, Heyne S, Dündar F, Manke T. 2016. deepTools2: a next generation web server for deep-sequencing data analysis. *Nucleic Acids Res* **44**: W160–W165. doi:10.1093/nar/gkw257
- Rosen BD, Bickhart DM, Schnabel RD, Koren S, Elsik CG, Tseng E, Rowan TN, Low WY, Zimin A, Coudrey C, et al. 2020. De novo assembly of the cattle reference genome with single-molecule sequencing. *Gigascience* **9**: gaaa021. doi:10.1093/gigascience/gaaa021
- Salimullah M, Mizuho S, Plessy C, Carninci P. 2011. NanoCAGE: a high-resolution technique to discover and interrogate cell

- transcriptomes. *Cold Spring Harb Protoc* **2011**: pdb.prot5559. doi:10.1101/pdb.prot5559
- Takahashi H, Lassmann T, Murata M, Carninci P. 2012. 5' end-centered expression profiling using cap-analysis gene expression and next-generation sequencing. *Nat Protoc* **7**: 542–561. doi:10.1038/nprot.2012.005
- Tav C, Tempel S, Poligny L, Tahi F. 2016. miRNAfold: a web server for fast miRNA precursor prediction in genomes. *Nucleic Acids Res* **44**: W181–W184. doi:10.1093/nar/gkw459
- Tong C, Chen Q, Zhao L, Ma J, Ibeagha-Awemu EM, Zhao X. 2017. Identification and characterization of long intergenic noncoding RNAs in bovine mammary glands. *BMC Genomics* **18**: 468. doi:10.1186/s12864-017-3858-4
- Van Eenennaam AL, Weigel KA, Young AE, Cleveland MA, Dekkers JCM. 2014. Applied animal genomics: results from the field. *Annu Rev Anim Biosci* **2**: 105–139. doi:10.1146/annurev-animal-022513-114119
- Wade JT, Grainger DC. 2014. Pervasive transcription: illuminating the dark matter of bacterial transcriptomes. *Nat Rev Microbiol* **12**: 647–653. doi:10.1038/nrmicro3316
- Weikard R, Hadlich F, Kuehn C. 2013. Identification of novel transcripts and noncoding RNAs in bovine skin by deep next generation sequencing. *BMC Genomics* **14**: 789. doi:10.1186/1471-2164-14-789
- Wucher V, Legeai F, Hédan B, Rizk G, Lagoutte L, Leeb T, Jagannathan V, Cadieu E, David A, Lohi H, et al. 2017. FEELnc: a tool for long non-coding RNA annotation and its application to the dog transcriptome. *Nucleic Acids Res* **45**: e57. doi:10.1093/nar/gkw1306
- Yamashita R, Sathira NP, Kanai A, Tanimoto K, Arauchi T, Tanaka Y, Hashimoto S-I, Sugano S, Nakai K, Suzuki Y. 2011. Genome-wide characterization of transcriptional start sites in humans by integrative transcriptome analysis. *Genome Res* **21**: 775–789. doi:10.1101/gr.110254.110

Received June 12, 2020; accepted in revised form February 1, 2021.